Effects of Three-Dimensional Roughness Elements on Boundary-Layer Transition and Aerodynamic Heating

MICHAEL G. DUNN*
Lockheed Missiles and Space Company, Sunnyvale, Calif.

In this investigation a dense array of 0.090-in. protruding rivets installed on the cylindrical section of a Lockheed Agena is considered. For comparison purposes, flush-rivet panels and protruding-rivet panels were instrumented for each flight. The downstream propagation of boundary-layer disturbances resulting from the presence of the roughness elements is also described. Presence of the roughness elements prolongs the existence of the turbulent boundary layer. Local transition Reynolds numbers for the roughened surface may be reduced to one-third the value for the corresponding smooth surface. Within the data accuracy, the roughness elements did not influence the turbulent flow heat-transfer coefficients.

Nomenclature

h = local heat-transfer coefficient
M = Mach number
Nu = Nusselt number
Pr = Prandtl number
$\dot{q}$ = heat rate
Re = local Reynolds number
T = absolute temperature
x = wetted distance from stagnation point
δ^* = boundary-layer displacement thickness
μ = dynamic viscosity
ρ = density
θ = boundary-layer momentum thickness

Subscripts

e = evaluated at local edge of boundary-layer conditions
w = evaluated at wall conditions
$*$ = evaluated at Eckert reference temperature
∞ = evaluated at freestream conditions upstream of bow shock
lam = laminar flow

Introduction

FOR reasons of economy, the use of protruding fasteners on the external surfaces of satellite vehicles has been increasing. However, the deficiency of applicable experimental or flight data on the effects of protruding fasteners on the convective heat transfer has required a necessarily conservative approach in design predictions. Such protuberances may influence the convective heat-transfer calculation in two ways: by prolonging the presence of the turbulent boundary-layer heating pulse and thus increasing the total heat transfer, and by increasing the skin-friction coefficient and thus increasing the local heat-transfer rates.

In 1953 Dryden[1] reviewed the published data, with particular emphasis on a single roughness element on a flat plate, and found the transition Reynolds number to be a function of the ratio of the height of the roughness element to the local boundary-layer displacement thickness. Braslow[2] later reviewed data for distributed three-dimensional roughness elements and found that the roughness height required to promote transition could be correlated using a local Reynolds number based on roughness height and the local flow conditions at that height. Van Driest and co-workers[3–5] studied the effects of a single row of spherical roughness elements located approximately 6 in. from the apex of a 10° half-angle cone on boundary-layer transition at Mach numbers 1.9, 2.7, and 3.7. Experimentally determined heat-transfer coefficients[6–9] can also be used to predict the influence of roughness elements on the convective heat transfer. However, only the data of Bloom and Pallone[9] were for boundary-layer parameters similar to those for the present problem, but for this work a dense array of protuberances was not considered. Nikuradse[10, 11] performed extensive experiments in order to determine the effect of surface roughness on the fluid-flow resistance in circular pipes. By systematically varying the height of sand grains and pipe diameter, he was able to determine resistance laws with the sand grain height as a parameter. Schlichting[12] used Nikuradse's roughness correlation and determined experimentally values of equivalent sand roughness applicable to surfaces with 0.15-in. protuberances arranged in various patterns. Clutter[13] presents comprehensive charts for determining skin-friction coefficients for both smooth and rough flat plates for Mach numbers up to 5.0 with and without heat transfer.

Received March 13, 1963; revision received November 14, 1963. This work was performed, in part, under Air Force Contract AF04(647)-673.

* Associate Research Scientist, Launch and Entry Thermodynamics. Member AIAA.

Description of Experiment and Flight Data

The flight data described here provide some valuable extensions to the rather limited previous literature. The data were obtained from a series of three vehicles which will be denoted as Vehicles I, II, and III. Figure 1 presents a portion of a typical trajectory. Post-flight analysis indicated that the three vehicles did not perform identical pitch and yaw maneuvers. Vehicle I flew essentially a zero effective (combined pitch and yaw) angle-of-attack trajectory. The maximum effective angle-of-attack for Vehicle II was less than 6° and occurred after 120 sec. Vehicle III effective angles-of-attack were calculated to be somewhat greater than those of Vehicle II. The Nusselt-Reynolds number data indicate that prior to 120 sec after lift-off, Vehicle III pitch and yaw maneuvers had a negligible influence. Data after 120 sec are presented for completeness, but in obtaining these Nusselt-Reynolds number plots, the zero angle of incidence flow field was applied. Atmosphere parameters were obtained from the 1959 Air Research and Development Command.

Instrumentation consisted of silicon semiconductors (see Shearer[14] for discussion) located on the cylindrical section of the respective vehicle configurations, as shown in Fig. 2. A total of 33 sensors were flown on each vehicle with 25 on the protruding-rivet side (rivet pattern covered an area of 64 in.^{2} and rivets were installed in a square pattern on 2-in. centers) and 8 on the flush-rivets side. The sensors were ovalshaped, 0.09 × 0.04 in., and less than 0.0005 in. thick. The instrument has a rapid response and a very small thermal capacity

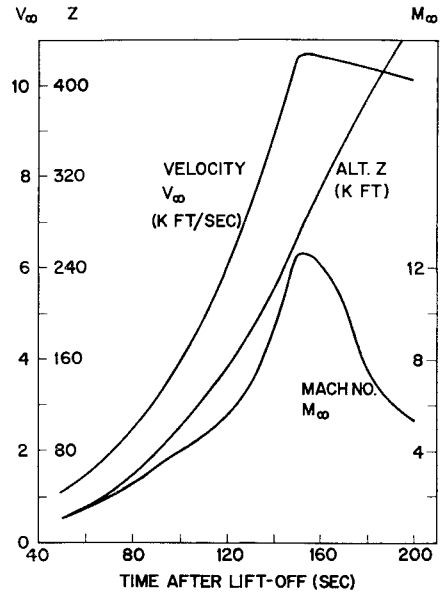

Fig. 1 Typical trajectory.

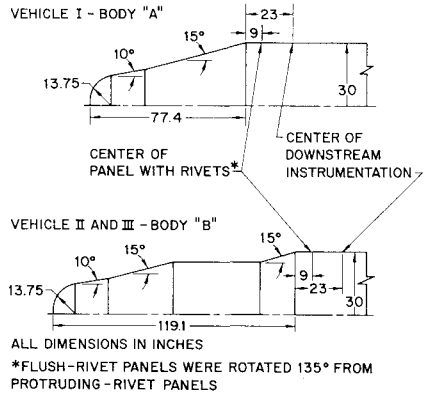

Fig. 2 Basic vehicle configurations.

compared to that of the skin. The quality of the flight data was fair for the first vehicle and good for the final two (Table 1).

Discussion

Transition Data

The inviscid flow surface pressure distributions used in the data reduction were obtained using a digital computer program, which is a combination of the Swigart[15] blunt-body solution and a method of characteristics solution developed by Benson.[16] A detailed description of the flow-field calculation procedure is presented by Lanfranco.[17] Figure 3 presents the time variation of the local Mach number and static pressure ratio for a point located on the stagnation point streamline midway between the upstream and downstream instrumentation for the Vehicle III configuration and trajectory.

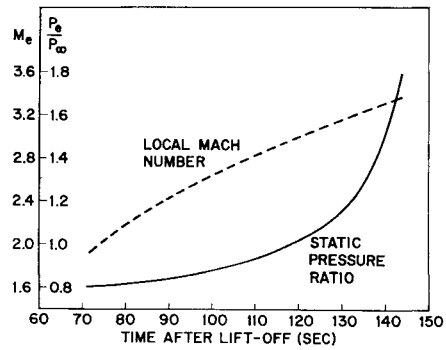

Fig. 3 Variation of local flow-field parameters.

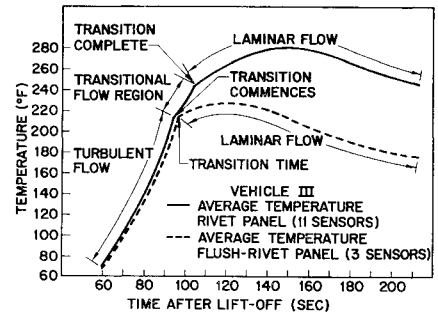

Fig. 4 Typical flight data showing transition, Vehicle III.

For clarification purposes, the technique used to determine boundary-layer transition is shown in Fig. 4. The transitional flow regime was observed for all three vehicles. However, it was difficult to establish the transitional regime bounds for Vehicle I due to the quality of the data. In Table 2 a summary of the local transition Reynolds number for each of the three flights is presented. For a given location and vehicle configuration, the local transition Reynolds number is essentially constant. Also presented in Table 2 are the free-stream Mach number, local Mach number, and wall to edge of the boundary-layer temperature ratio corresponding to the respective transition times.

Considering limiting values, it may be concluded that the roughened panel transition Reynolds number may be reduced to one-third the value for the corresponding flush-rivet panel, and that the effect of the roughness elements on boundary-layer transition was propagated downstream. The Nusselt-Reynolds number plots constructed using Vehicle III data indicate the presence of a transition region in which the flow is neither completely laminar nor completely turbulent. Transition occurred in a smaller Reynolds number region on the flush-rivet and downstream locations than it did on the corresponding protruding-rivet locations.

The compressible undisturbed laminar-flow momentum thickness θ_{lam} and displacement thickness δ^*_{lam} histories corresponding to the center of the riveted panels were computed using Monaghan's[18] technique. The computed variation of these parameters was then compared to the nominal protuberance height. A typical comparison is shown in Fig. 5. It is illustrated that transition to turbulent flow occurred

Table 1 Quality of flight data

Vehicle	Temperature range, °F	Band width (0–5ν) used	Sensor scatter, °F	Estimated error in transition time, sec	Over-all quality
I	0–550	30%	±5.0	±2.0	Fair
II	0–550	42%	±2.5	±1.5	Good
III	40–300	93%	±1.5	±1.0	Excellent

Table 2 Summary of transition Reynolds numbers

Vehicle	Location	Transition[a] time, sec	M_∞	M_e	T_w/T_e	Transition Reynolds number $Re_x \times 10^{-6}$	$Re_x^* \times 10^{-6}$	Re_θ
A) On riveted panel								
I	Flush	95	3.62	2.54	0.98	1.15	...	618
	Protruding	100	3.95	2.64	0.87	0.60	...	441
II	Flush	97	3.75	2.58	1.00	1.60	...	745
	Protruding	95	3.62	2.54	1.23	2.00	...	865
		107	4.40	2.77	0.78	0.47	...	406
III	Flush	98	3.82	2.60	1.00	1.85	1.32	860
	Protruding	95	3.62	2.54	1.27	2.60	1.83	930
		105	4.30	2.74	0.87	0.80	0.58	544
B) Downstream of riveted panel								
I	Flush	95	3.62	2.54	0.99	1.30	...	...
	Protruding	103	4.15	2.70	0.80	0.45	...	...
II	Flush	101	4.01	2.66	0.91	1.10	...	...
	Protruding	95	3.62	2.54	1.19	2.00	...	...
		111	4.70	2.84	0.69	0.29	...	...
III	Flush	99	3.90	2.62	0.94	1.85	1.19	...
	Protruding	98	3.82	2.60	0.96	2.10	1.35	...
		113	4.85	2.88	0.66	0.33	0.234	

[a] Where two numbers appear, times indicate onset and completion of transition, respectively.

when θ_{lam} was approximately equal to the protuberance height. The corresponding momentum thickness Reynolds numbers Re_{θ_t} were between 400 and 550. This result should be helpful for estimating boundary-layer transition for future problems of this nature.

Heat-Transfer Data

A simple thin-skin analysis (skin thickness was a nominal 0.071-in. magnesium) was used to calculate the convective heat-transfer rates (see Appendix A) from the temperature-time flight data of Vehicle III. Instantaneous heat-transfer rates were calculated for each sensor. The corresponding instantaneous heat rates for a particular instrumented section were then averaged and used to calculate the respective heat-transfer coefficients and Nusselt numbers. Averaged instantaneous heat rates for the respective locations are compared in Figs. 6 and 7. Nusselt-Reynolds number comparisons for the respective locations are given in Figs. 8 and 9. The Nusselt number presentations are based on properties evaluated at the Eckert[19] reference temperature. Familiar local flat-plate Nusselt number correlations are also presented on Figs. 8 and 9.

It may be concluded from Fig. 8 that the turbulent flow local flat-plate theory agrees favorably with the roughened surface Nusselt number data for Reynolds numbers greater than 2×10^5, and the flush-rivet surface Nusselt number data for Reynolds numbers greater than 8×10^5. Further, the flush-rivet surface Nusselt number data agree favorably with laminar flow local flat-plate theory in the Reynolds number range 7×10^4 to 2×10^5. At Reynolds numbers less than 7×10^4, vehicle maneuvers commence to influence the results. The data are presented for the purposes of completeness, but one may recall that the zero angle of incidence flow field was used in the reduction. National security precludes the release of a time history of the vehicle maneuvers.

Similar conclusions can be drawn from Fig. 9. Turbulent flow local flat-plate theory agrees favorably with the Nusselt number data downstream of the roughened panel for Reynolds numbers greater than 1×10^5, and the Nusselt number data downstream of the flush-rivet surface for Reynolds numbers greater than 5×10^5. Nusselt number data downstream of the flush-rivet surface agree favorably with laminar flow flat-plate theory in the Reynolds number range 7×10^4 to 3×10^5. Once again, vehicle maneuvers become significant at Reynolds numbers less than 7×10^4. Data accuracy for the flush-rivet and corresponding downstream results at Reynolds numbers less than 7×10^4 is somewhat questionable, since the respective convective heat rates were less than 0.1 Btu/ft^2-sec.

Within the accuracy of the flight data, it is not possible to distinguish a difference between the turbulent-flow Nusselt numbers of the protruding and flush-rivet panels. Indications are that the roughness elements had a negligible effect

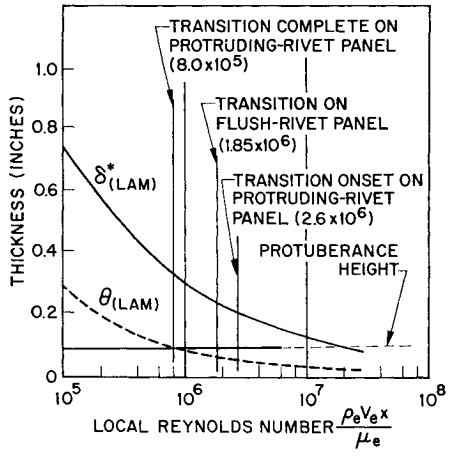

Fig. 5 Predicted laminar flow momentum and displacement thickness. Vehicle III.

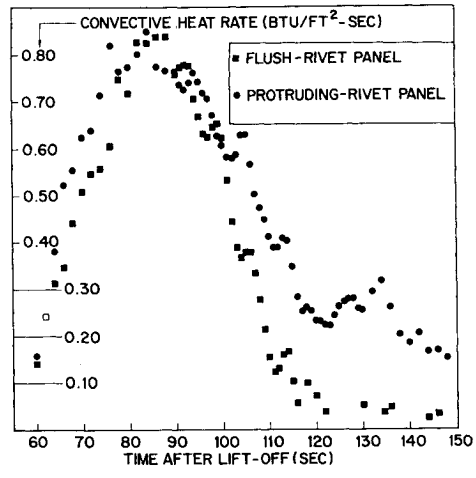

Fig. 6 Convective heat rates for riveted panels, Vehicle III.

on the magnitude of the turbulent-flow heat-transfer coefficients.

Conclusions

Significant conclusions based on the flight data presented are as follows:

1) The presence of the turbulent boundary-layer was prolonged significantly due to the presence of the surface protuberances.

2) The disturbance resulting from the presence of the roughness elements was propagated downstream.

3) Transition was completed on the roughened surface when the laminar boundary-layer momentum thickness was approximately equal to the protuberance height.

4) Good agreement between Nusselt numbers calculated using flight data and predicted Nusselt numbers can be shown for the smooth surfaces.

5) The roughness elements investigated had a negligible influence on the magnitude of the turbulent-flow heat-transfer coefficients.

Appendix A

Data Reduction

A simple thin-skin analysis including convection, internal radiation, and external radiation was utilized to calculate the surface heat flux. Preflight measurements of skin thickness and photographs of the installation were obtained to aid in the data reduction. The thermal model assumed that energy exchange could occur only at the external and internal surfaces. During the time interval for which significant data are reported (60–120 sec) substructure conduction was negligible and thus neglected. Convective heat rates were calculated from Eq. (1):

$$\dot{q}_{conv} = \rho C_p \delta \frac{dT_w}{d\tau} + 0.4761 \times 10^{-12}[\epsilon_{ext}\{(T_w)^4 - (T_s')^4\} + \epsilon_{int}\{(T_w)^4 - (T_s)^4\}] \quad \text{(A1)}$$

where T_s' is the space sink temperature calculated to be 455°R from the relationship[20]:

$$\sigma\epsilon_{ext}(T_s')^4 = \alpha_s[F_s S + F_r R] + \epsilon_{ext} F_e E \quad \text{(A2)}$$

where

σ = Stefan-Boltzmann constant
α_s = solar absorptivity
ϵ_{ext} = external surface emissivity
ϵ_{int} = internal surface emissivity
T_s = internal radiation temperature assumed to be 500°R
F_e, F_r, F_s = view factors between surface and earth, surface and reflected solar, and surface and direct solar radiation, respectively
S = solar radiation intensities
E = earth radiation intensity

In order to avoid bias, the data reduction was performed by a digital computer. An 11-point smoothing technique was applied to the telemeter data to obtain the instantaneous temperature-time derivatives $dT_w/d\tau$ used in Eq. (1).

Convective heat-transfer coefficients were calculated from

$$\dot{q}_{conv} = h(T_r - T_w) \quad \text{(A3)}$$

where $\dot{q}_{conv}$ is the arithmetic average of the instantaneous heat rates; T_r is the recovery temperature computed using $(Pr^*)^{1/3}$ for the turbulent flow recovery factor and $(Pr^*)^{1/2}$ for the

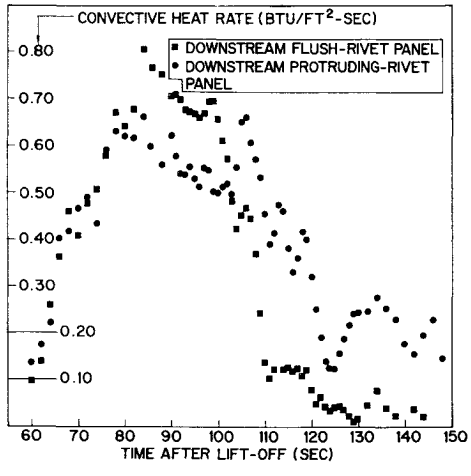

Fig. 7 Convective heat rates downstream of riveted panels, Vehicle III.

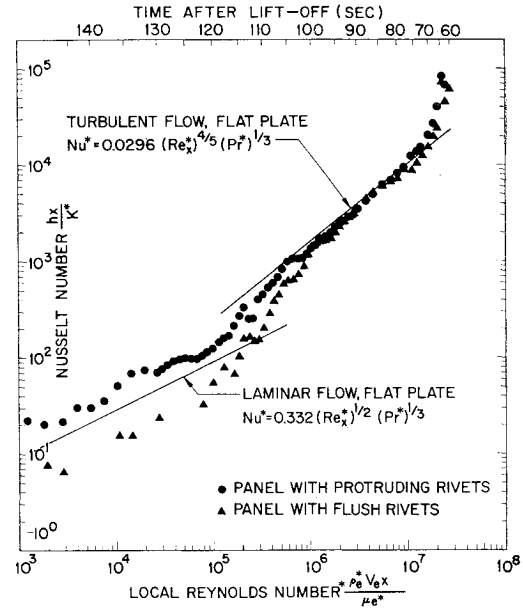

Fig. 8 Comparison of observed and predicted Nusselt numbers for riveted panels, Vehicle III.

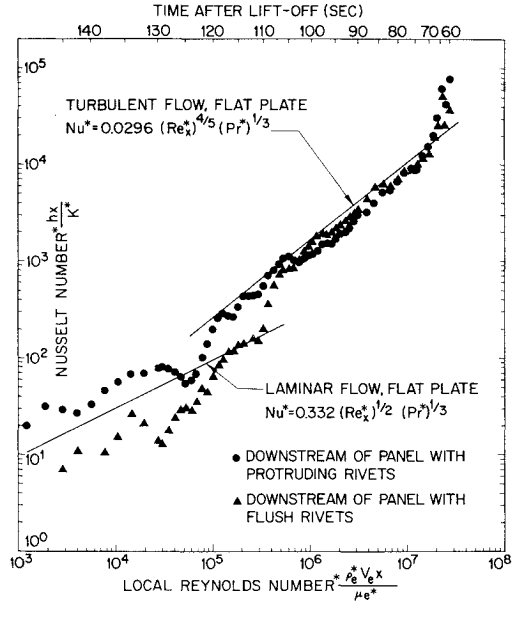

Fig. 9 Comparison of observed and predicted Nusselt numbers downstream of riveted panels, Vehicle III.

laminar flow recovery factor, and $\gamma = 1.4$; T_w is evaluated from flight data, T_e and M_e are evaluated using the previously described flow field and the 1959 Air Research and Development Command Atmosphere. Prior to 90 sec after lift-off the average values of the heat rates were computed at 2 sec intervals. Between 90 and 140 sec the averages were computed at 1-sec intervals.

Real gas effects were assumed to be negligible for the purposes of data reduction. This assumption was justified, since the Eckert reference temperature reached a maximum value of approximately 2800°R during the time interval for which data are reported.

References

[1] Dryden, H. L., "Review of published data on the effect of roughness on transition from laminar to turbulent flow," J. Aeronaut. Sci. **20,** 477–482 (1953).

[2] Braslow, A. L., "Review of the effect of distributed surface roughness on boundary-layer transition," AGARD Rept. 254 (1960).

[3] Van Driest, E. R. and Blumer, C. B., "Effect of roughness on transition in supersonic flow," Air Force Off. Sci. Res., TN 60-1164 (1960).

[4] Van Driest, E. R. and McCauley, W. D., "The effect of controlled three-dimensional roughness on boundary-layer transition at supersonic speeds," J. Aerospace Sci. **27,** 261–271 (1960).

[5] Van Driest, E. R. and Boison, J. C., "Experiments on boundary layer transition at supersonic speeds," J. Aerospace Sci. **24,** 885–899 (1957).

[6] Wisniewski, R. J., "Turbulent heat-transfer coefficients in the vicinity of surface protuberances," NASA Memo 10-1-58E (1958).

[7] Burbank, P. B. and Strass, H. K., "Heat transfer to surfaces and protuberances in a supersonic turbulent boundary layer," NASA RM L58E01a (1958).

[8] Mitchell, W. B., Radcliffe, W. R., Yip, P. S., and Wentink, R. S., "Summary report for the aerodynamic heating test at the NASA Langley unitary plan wind tunnel," Rept. no. AE60-0574, Contract no. AF04(647)-4, Convair/Astronautics (1960).

[9] Bloom, M. H. and Pallone, A., "Heat transfer to surfaces in the neighborhood of protuberances in hypersonic flow," Polytechnic Inst. Brooklyn, Wright Air Dev. Center, TN 57-95 (1957).

[10] Nikuradse, J., "Gesetzma Bigkeiten der Turbulenten Stromung in Glatten Rohren," Forsch. Arb. Ing. Wesen, no. 356 (1932).

[11] Nikuradse, J., "Turbulente Stromung in nicht Kreisformigen Rohren," Ing. Arch 1, 306 (1930).

[12] Schlichting, H., "Experimentelle Untersuchungen zum Rauhigkeitsproblem," Ing. Arch. **7,** 1 (1936); Eng. Trans. in Proc. Am. Soc. Mech. Engrs. (1936).

[13] Clutter, D., "Charts for determining skin-friction coefficients on smooth and rough flat plates at Mach numbers up to 5.0 with and without heat transfer," Douglas Aircraft Co., Rept. ES 29074 (1959).

[14] Shearer, C. R., "Semi-conductor temperature sensors," Instrument Society of America, Preprint 159-LA-61 (1961).

[15] Swigart, R. J., "A theory of asymmetric hypersonic blunt-body flows," Inst. Aerospace Sci. Paper 62-98 (June 1962).

[16] Benson, J. L., "The method of characteristics and its application to digital computer solutions of some supersonic flow problems," Lockheed California Div., Rept. 13606 (October 1959).

[17] Lanfranco, M. J., "A solution to the supersonic flow past blunt bodies of revolution," TM 5341-17, Lockheed Missiles and Space Co. A362449 (November 1963).

[18] Monaghan, R. J., "An approximate solution of the compressible laminar boundary layer on a flat plate," R & M, No. 2760, British Ames Research Center (1953).

[19] Eckert, E. R. G., "Survey of boundary layer heat transfer at high velocities and high temperatures," Wright Air Dev. Center TR 59-624 (1960).

[20] Camack, W. G. and Edwards, D. W., "Effect of surface thermal-radiation characteristics on the temperature control problem in satellites," First Symposium, *Surface Effects on Spacecraft Materials,* edited by F. Clauss (John Wiley and Sons, Inc., New York, 1960), pp. 3–54.